Iterative two-dimensional signal warping—Towards a generalized approach for adaption of one-dimensional signals

Martin Schmidt[a,*], Mathias Baumert[b], Hagen Malberg[a], Sebastian Zaunseder[a]

[a] *Institute of Biomedical Engineering, TU Dresden, Dresden, Saxony, Germany*
[b] *School of Electronics and Electrical Engineering, University of Adelaide, Adelaide, South Australia, Australia*

1. Introduction

Extracting quasi-periodic features from noisy signals is a common challenge in the field of biomedical signal processing. To track beat-to-beat changes in cardiovascular variables over time, template matching algorithms have evolved [1–3]. A widely used technique to determine beat-to-beat changes of QT intervals relies on homogeneously stretching the ST-T segment of the beat under consideration until it matches best a ST-T template [1]. To consider temporal changes of the QRS complex the time shifting algorithm has been introduced [2]. The main idea is to construct separate QRS and T wave templates and shift them in time to determinate the QT interval. From a physiological point of view, these techniques might not be able to capture all morphological changes within the QT interval.

The description of subtle morphological changes in electrocardiograms (ECG) may yield novel risk factors for cardiac mortality [4,5], but the low signal to noise ratios imposes practical challenges. To address these issues, we introduced a technique that adapts one-dimensional (1D) templates in a two-dimensional (2D) manner, so-called two-dimensional signal warping (2DSW) in 2014 [3]. A 2D mesh superimposed on the signal, allows subtle segmentation of the template taking into account inhomogeneous variations of waveform morphologies.

Several clinical research studies and multiple systematic investigations have demonstrated the power of 2DSW in applications related to QT variability (QTV) assessment [6–11]. We further proposed a simple formula to correct for the inverse relationship between QTV and T wave amplitude. Using this correction, predictive value of QTV for all-cause mortality in patients with non-ischemic cardiomyopathy has been demonstrated [11]. Nevertheless, analysis of long-term ECG recordings showed limitations of 2DSW to adapt to large shape variations, e.g. caused by circadian rhythm [6]. These limitations in the template adaptation are mainly due to the fixed 2D mesh segmentation. As a consequence, we further developed 2DSW, referred to as iterative 2DSW (i2DSW), to remove these limitations. With respect to the enhancements of

* Corresponding author.
E-mail addresses: martin_schmidt@tu-dresden.de (M. Schmidt), mathias.baumert@adelaide.edu.au (M. Baumert), hagen.malberg@tu-dresden.de (H. Malberg), sebastian.zaunseder@tu-dresden.de (S. Zaunseder).

i2DSW, we were faced with the tradeoff between generalization of the technique for all quasi-periodic signals on the one hand, and achievement of robust and sensitive results in the application of QTV measurement on the other hand.

This article is structured as follows: Section 2 covers a summary of the 2DSW warping concept published in [3]. The iterative implementation and generalization of 2DSW is introduced in Section 3. Section 4 applies the iterative 2DSW algorithm to waveform variability assessment in ECG and QTV evaluation, in particular using simulated and real data. The results are shown in Section 5. Section 6 discusses i2DSW in comparison to standard 2DSW and common algorithms.

2. Warping concept

2DSW [3] aims to adapt a template to a waveform by minimizing the distance between both. This is realized by superimposing a 2D mesh of warping points on the template to be adapted. The 2D mesh, the so-called warping grid, is built of N_C columns and N_R rows. Each intersection defines a warping point P_i with $i = 1, 2, \ldots, N_P$, where N_P is the number of warping points in the warping grid. The area spanned by a quadrangle of four warping points is called warping area, denoted as A. Warping points are active warping points $P^{(1)}$, if at least one of the up to four surrounding areas contains part of the template to be adapted. Otherwise, these warping points are denoted as passive warping points $P^{(0)}$. To modify the template in A, a 2D shift of one or more adjacent active warping points is necessary. Each absolute coordinate of the template $[x, y] \in A$ has a relative coordinate $[x^{(rel)}, y^{(rel)}]$, see Fig. 1. Each relative position remains unchanged in the 2DSW deforming process, so that all template coordinates $[x, y] \in A_j$ with $j = 1, 2, \ldots, N_A$, where $N_A = (N_C - 1) \cdot (N_R - 1)$ is the total number of areas in the warping grid, belong to an warping area A_j. Thus, a drift of template coordinates to neighboring areas is not possible. The template adaption is achieved by minimizing the euclidean distance

$$d^{(2n)}(Y^{(1)}, Y^{(2)}) = \frac{\sqrt{\sum_{l=1}^{|\mathcal{Y}|} \left(y_l^{(1)} - y_l^{(2)}\right)^2}}{|\mathcal{Y}|} \tag{1}$$

between template $\mathcal{Y}^{(1)}$ and waveform $\mathcal{Y}^{(2)}$ normalized by the signal length $|\mathcal{Y}|$. The signals $\mathcal{Y}$ are defined as a set of vectors $[x, y]$, $\mathcal{Y} = \{[x, y]| \in \mathbb{R} \times \mathbb{R}\}$. X and Y represent the series of x and y values. To compute $d^{(2n)}(Y^{(1)}, Y^{(2)})$, the domains $X^{(1)}$ and $X^{(2)}$ have to be identical, otherwise interpolation/resampling is applied. The shifting of warping points underlies two constraints: (1) the functional character of the template has to be preserved, i.e. each x value has one single corresponding y value. (2) The maximum of the two-dimensional shift is restricted in x and y direction. This prevents warping areas from reducing below a given size or cut across neighboring areas. In the original design 2DSW is implemented by applying a predefined warping grid to adapt the waveform (further details are given in [3]). The parameterization of this grid involves limitations in the deforming process. To remove the limits an iterative 2DSW algorithm is proposed in the following section.

3. Iterative implementation

3.1. Iterative generalization

Iterative two-dimensional signal warping realizes the basic concept of 2DSW by applying a divide and conquer strategy. By repeating 2DSW multiple times, starting with a warping grid of a single warping area A and refining that grid in each iteration *iter*, a stepwise template adaption is realized. The refinement of the warping grid is implemented by dividing each warping area in subareas, illustrated in Fig. 2. Because macroscopic morphological adjustments can be made in the first iteration, passive shifting of

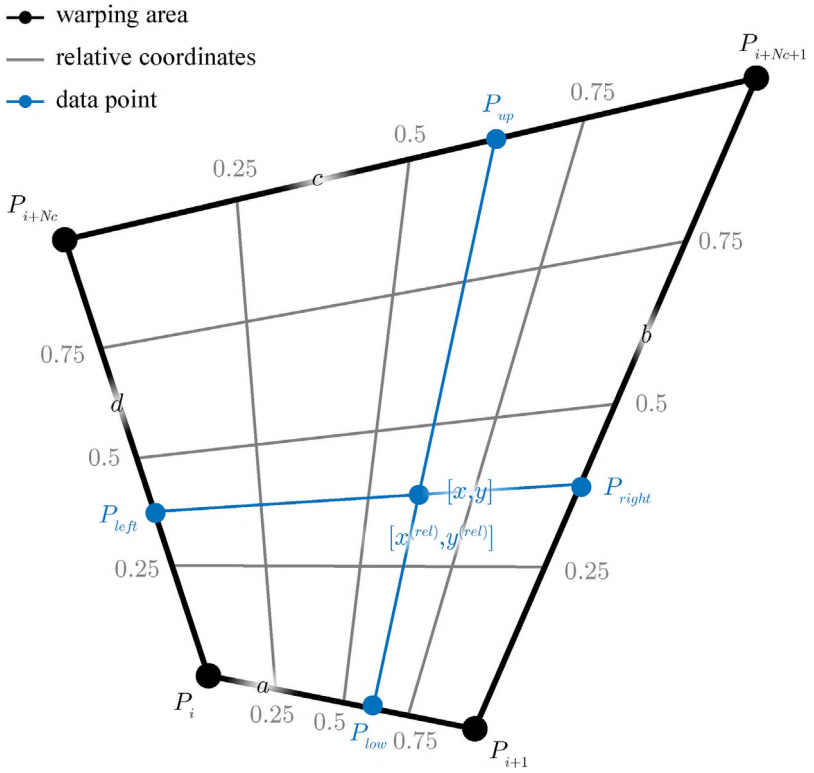

Fig. 1. Illustration of the relative position $[x^{(rel)}, y^{(rel)}]$ of an arbitrary point in a non-rectangular warping area. Four warping points P_i spawn a warping area. The borders are denoted as vectors a, b, c and d.

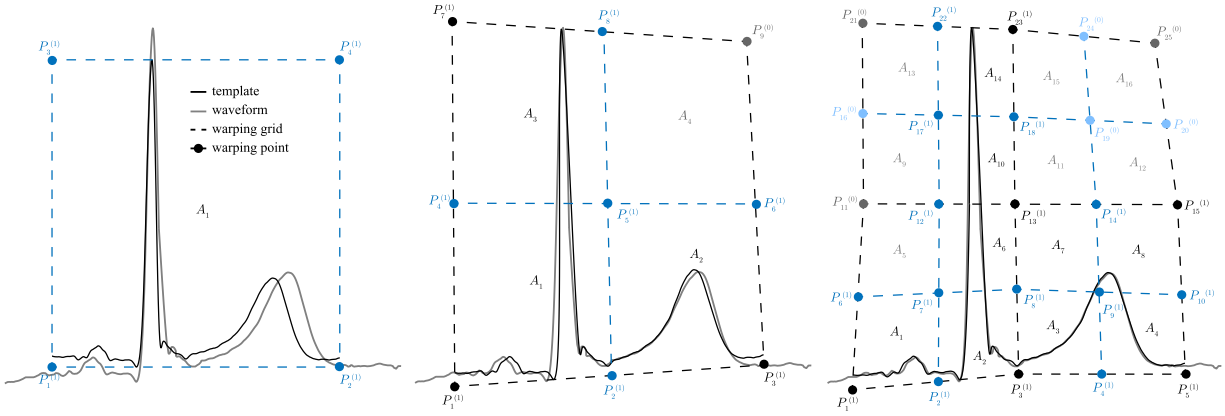

(a) warping grid for iteration 1. (b) warping grid for iteration 2. (c) warping grid for iteration 3.

Fig. 2. Iteration schematic of i2DSW exemplary for three iterations. (a) Shows the warping grid with the initialized unwarped ECG template. The warping grid in iteration 1 is composed of one warping area A_1. After shifting all active warping points $P_i^{(1)}$, the number of segments is doubled in each direction in the next iteration. The new warping grid for iteration 2 is illustrated in (b). In (c) the adapted warping grid of iteration 2 is shown with the new segment preparation for iteration 3. Active warping points added in the new iteration are colored in blue, passive warping points added in the new iteration are colored in light blue, previously added active warping points are colored in black, previously added passive warping points are colored in gray. (For interpretation of the references to color in this figure legend, the reader is referred to the web version of this article.)

warping points, which occurs in the original 2DSW implementation is avoided. In contrast, with each iteration the template $\mathcal{Y}$ is adapted more subtly. The iteration process is denoted as

$$\dot{\mathcal{Y}}, \ddot{\mathcal{Y}}, \ldots, \overset{(iter_{\max})}{\mathcal{Y}}$$

where $\cdot, \cdot\cdot, \ldots, iter_{max}$ denotes the iteration cycle. The final adaption in the last iteration $iter_{max}$ is termed as $\mathcal{Y}'$. By increasing the number of warping points N_P in each iteration, the warping sections of the template in the warping areas get smaller and can therefore be adapted more flexibly. To avoid overadaptation two constraints are considered. First, the maximum shift $\boldsymbol{s}_i^{(\max)}$ of warping points P_i that is allowed in x and y direction, can be adjusted in each iteration. This is used to prevent warping points from crossing neighboring warping areas, because the distance to the neighbored area is shortening in each iteration. Second, the euclidean distance $d^{(2n)}$ in each iteration cycle

$$d^{(\dot{2}n)}, d^{(\ddot{2}n)}, \ldots, \overset{(iter_{\max})}{d^{(2n)}}$$

is monitored. If $\overset{(iter)}{d^{(2n)}}$ exceeds a predefined threshold from *iter* to *iter* + 1, the iteration procedure is stopped. This aims at reducing the influence of fluctuations that would deform the warping grid by adapting small waveform variations that may be predominately caused by signal noise.

3.2. Warping point processing

The basic idea is to shift those warping points first that have the largest impact. For each warping point the distance between template and waveform is calculated. Next, warping points are sorted by descending distance to obtain a *warping point sequence*

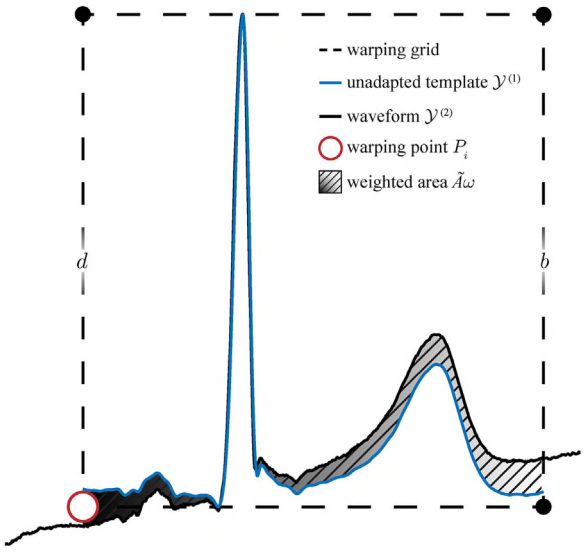

Fig. 3. Illustration of warping point related weighted distance area $\tilde{A}\omega$ calculation. The warping point under consideration is in the left lower corner. $\tilde{A}$, i.e. the area between unadapted template $\mathcal{Y}^{(1)}$ and waveform $\mathcal{Y}^{(2)}$ is weighted by the two-dimensional relative distance of each $[x, y] \in \tilde{A}$ to the considered warping point P_i. $\tilde{A}\omega(x, y)$ is colored from black ($\tilde{A}\omega(x, y) = 1$) to white ($\tilde{A}\omega(x, y) = 0$). (For interpretation of the references to color in this figure legend, the reader is referred to the web version of this article.)

$\mathcal{S}$, illustrated in Fig. 3. First, the area $\tilde{A}$ between template $\mathcal{Y}^{(1)}$ and waveform $\mathcal{Y}^{(2)}$ is calculated as

$$\begin{aligned}\tilde{A} = \{\,[x,y] \quad \in \mathbb{R}^2 |\\ y \quad &\geq \min(\mathcal{Y}^{(1)}(X^{(1)}=x), \mathcal{Y}^{(2)}(X^{(2)}=x)) \wedge \\ y \quad &\leq \max(\mathcal{Y}^{(1)}(X^{(1)}=x), \mathcal{Y}^{(2)}(X^{(2)}=x)) \wedge \\ x \quad &\geq d_x \left(\frac{|y-y_i|}{|y_{i+N_c}-y_i|} \right) \wedge \\ x \quad &\leq b_x \left(\frac{|y-y_{i+1}|}{|y_{i+N_c+1}-y_{i+1}|} \right) \Bigg\},\end{aligned} \tag{2}$$

where $\mathcal{Y}(X = x)$ returns the corresponding y value of the vector $[x, y] \in \mathcal{Y}$.

$$\tilde{A}(x, y) = \begin{cases} 1 & |[x, y] \in \tilde{A}, \\ 0 & |[x, y] \notin \tilde{A}. \end{cases} \tag{3}$$

Second, a weight factor ω for each vector $[x, y]$ is calculated as

$$\omega(x, y) = (1 - x^{(rel)}) \cdot (1 - y^{(rel)}). \tag{4}$$

Thus, vectors $[x, y]$ close to the warping point under consideration are weighted higher than vectors further away. The weighting accounts for the fact that areas closer to the warping points are stronger affected by displacements of the respective warping point. By multiplying the area $\tilde{A}$ with ω, the weighted distance area between template and waveform is given.

$$\tilde{A}\omega(x, y) = \tilde{A}(x, y) \cdot \omega(x, y). \tag{5}$$

For every warping point P_i, the weighted distance is computed as

$$\Omega_i = \sum_{[x,y] \in \tilde{A}\omega} \tilde{A}\omega(x, y). \tag{6}$$

If the warping grid contains more than one area A_j, $\tilde{A}$ is divided into different areas $\tilde{A}_j$ by the warping grid. Ω_i is calculated as

$$\Omega_i = \sum_{j \in N_n^i} \sum_{[x,y] \in \tilde{A}_j\omega} \tilde{A}_j\omega(x, y), \tag{7}$$

where N_n^i are the indexes of neighbor areas to the warping point P_i. The sequence of all Ω_i sorted in descending order is the so-called warping point sequence $\mathcal{S}$. The sequence defines the execution order of all warping points P_i.

3.3. Algorithmic implementation

The proposed heuristic solution is shown in Algorithm 1. The heuristic procedure does not guarantee optimal matching, but empirical analyses suggest the method to produce satisfactory results in adequate computational time. To reduce the processing time, x and y shifts s_x and s_y of each warping point P_i are executed in parallel. Because of the mathematically independent operations, this has no impact on the algorithmic solution but reduces computing time for CPUs with multiple cores. The 2DSW fast search optimization to find the optimal shift $\boldsymbol{s_i}$ remains unchanged. The fast search avoids computing all possibilities of shifts to find the optimal shift $\boldsymbol{s}_o$. By evaluating a grid of 5×5 extreme shifts the range of $\boldsymbol{s}_o$ is circumscribed. This procedure is iteratively repeated until the range of $\boldsymbol{s}_o$ cannot be further minimized [3].

Algorithm 1. Heuristic solution to i2DSW

Input: Template $\mathcal{Y}^{(1)}$, waveform $\mathcal{Y}^{(2)}$

while $iter < iter_{max}$ **do**
  Define warping points $\mathcal{P}$;
  Assign waveform to areas $\rightarrow \mathcal{Y}_j^{(1)}$;
  Calculate warping point sequence $\mathcal{S}$;
  for $o = 1, 2, \ldots, N_S$ **do**
    if $\mathcal{S}_o \in \mathcal{P}^{(1)}$ **then**
      Apply fast search to find optimal shift $\boldsymbol{s}_o$;
      Do shifting by $\boldsymbol{s}_o$ $(P_o \rightarrow P'_o)$;
    end
  end
  Check iteration break conditions;
  Increment$(iter)$;
end

Output: $\mathcal{Y}^{(1)\prime}$

4. Application to ECG waveform variability assessment

4.1. General framework

The general framework for ECG processing described in [3] was retained unchained. To reuse implementations of other algorithms (e.g. biosig toolbox [12]) the general framework is implemented in MathWorks MATLAB. The mathematical solution is implemented in C++. Fig. 4 shows the general scheme of QT variability calculation using i2DSW. The specific adaptions for the iterative generalization are detailed in the following sections. Briefly, real ECG raw data are filtered by using a digital butterworth high pass filter (filter order 30, cut-off requency 0.3 Hz). QRS locations are detected by applying the algorithm by Afonso et al. [13] implemented in the biosig toolbox [12]. ECG annotations are adjusted by time delay estimation (TDE) [14]: for each beat i, an aligned beat location $t_{QRS,i}$ is calculated by optimizing the joint similarity. PT segments that contain the entire waveform of a cardiac cycle are extracted respective to Eq. (8), introduced in Section 4.2. The template is constructed by averaging PT segments of the beats occurring in a window of 100 s in the first 30 min of a record. By searching for the 100 s window with the most similar waveforms, signal quality is considered and a smooth template is constructed. Fiducial points in the template are calculated semi-automatically in the template delineation procedure by applying the method of Laguna et al. [15]. The warping grid segmentation is linear and initialized with the template in x and y-direction, starting with one warping area ($N_A = 1$). The number of areas increases on each iteration cycle, details are descriped in Section 4.3.

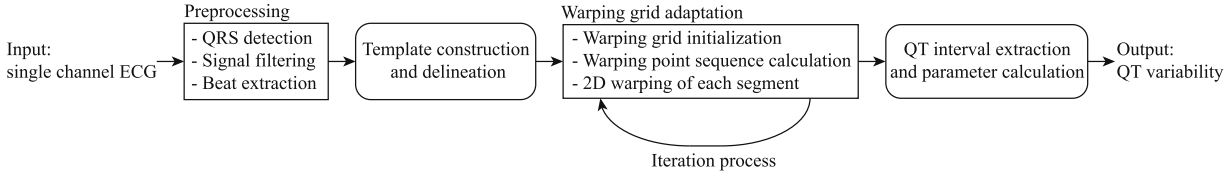

Fig. 4. General scheme of QT variability using i2DSW. Boxed items indicate processing steps.

4.2. Template definition

Whereas 2DSW was introduced to measure variability in the QT segment of the ecg waveform, i2DSW is applied to the PQ waveform. Therefore, preprocessing steps i.e. template construction, template delineation and grid preparation are extended to the PQ segment. Based on Laguna et al. [16] the beat window for beat i is calculated as

$$t_{\mathrm{Pon},i} = t_{QRS,i} - 370\,ms$$

$$t_{\mathrm{Tend},i} = \begin{cases} t_{QRS,i+1} - 240\,ms, & \bar{RR} \geq 720\,ms \\ t_{QRS,i} + \frac{2}{3}\bar{RR}, & \bar{RR} < 720\,ms \end{cases}, \tag{8}$$

where $t_{Pon,i}$ represents the beginning and $t_{Tend,i}$ the end of the PT segment; $\bar{RR}$ represents the mean RR-interval over all beats, $t_{QRS,i}$ the QRS location of beat i. Eq. (8) was chosen because it extends the QT window about 200 ms for the approximated maximum length of PQ segment [17].

4.3. Iteration process

In each iteration cycle the template is adapted more subtly by refining the warping grid. The segmentation is linear in x- and y-direction. Starting with one warping area $\dot{N}_A = 1$, the number of segments in x- and y-direction doubles ($iter > 1$):

$$\overset{(iter)}{N_A} = 2 \cdot \left(\overset{(iter-1)}{N_C} - 1 \right) \cdot 2 \cdot \left(\overset{(iter-1)}{N_R} - 1 \right) = 4 \cdot \overset{(iter-1)}{N_A}. \tag{9}$$

The maximum number of iterations $iter_{max}$ was set to 4. This value is chosen empirically to allow for template segmentation of i2DSW $\left(\overset{(4)}{N_A} = 64 \right)$ that is comparable to that of 2DSW ($N_A = 28$) on one hand and avoid over adaptations on the other hand (the fifth iteration $\left(\overset{(5)}{N_A} = 256 \right)$ tends to adapt signal noise). Together with the fast search optimization (see Section 3.3), the limitation of the maximum number of iterations $iter_{max}$ ensures the convergence and termination of i2DSW.

The higher the iteration cycle, the smaller the expected adaptations. Therefore, and to minimize the progressing complexity, the maximal shift $\boldsymbol{s}_i^{(\max)}$ is minimized in each iteration cycle as

$$\overset{(iter+1)}{\boldsymbol{s}_i^{(\max)}} = 0.5 \cdot \overset{(iter)}{\boldsymbol{s}_i^{(\max)}}, \tag{10}$$

where i is the specific warping point. For long-term recordings, the condition is applied beginning with the second iteration. To consider the convergence of $\overset{(iter)}{d^{(2n)}}$, the difference $\overset{(iter)}{\Delta d^{(2n)}}$ and ratio $\overset{(iter)}{\Phi d^{(2n)}}$ between the current and last iteration cycle are calculated as

$$\overset{(iter)}{\Delta d^{(2n)}} = \overset{(iter-1)}{d^{(2n)}} - \overset{(iter)}{d^{(2n)}} \tag{11}$$

$$\overset{(iter)}{\Phi d^{(2n)}} = \frac{\overset{(iter)}{d^{(2n)}}}{\overset{(iter-1)}{d^{(2n)}}}. \tag{12}$$

The parameter value to abort the iteration process before $iter_{max}$ has been reached is empirically defined as

$$\overset{(iter)}{\Delta d^{(2n)}} \leq \begin{cases} 0.100\ \mu\mathrm{V/sample} & iter = 1 \\ 0.050\ \mu\mathrm{V/sample} & iter = 2 \\ 0.025\ \mu\mathrm{V/sample} & iter = 3 \end{cases} \tag{13}$$

and

$$\overset{(iter)}{\Phi d^{(2n)}} \geq \begin{cases} 0.75 & iter = 1 \\ 0.85 & iter = 2 \\ 0.95 & iter = 3 \end{cases}. \tag{14}$$

If one of the aborting conditions is met the iteration process is aborted.

4.4. QTV quantification

For calculating QT interval QT_i of every beat i, iso-electric level ($Isolevel_i$) estimation and T wave amplitude $T_{i,amp}$ determination is necessary. Thereto, time (t) and amplitude (y) coordinates relating to the end of the P wave (*Pend*), Q wave (*Qonset*), the peak of the T wave (*Tpeak*) and its end (*Tend*) are extracted (the $Isolevel_i$ is defined as median value of the 'flattest' waveform segment (20 ms) between $t_{Pend,i}$ and $t_{Q,i}$ [18]):

$$QT_i = t_{Tend,i} - t_{Qonset,i} \tag{15}$$

$$T_{amp,i} = y_{Tpeak,i} - Isolevel_i \tag{16}$$

We used the standard deviation of QT intervals (SDQT) to quantify QTV:

$$SDQT = \sqrt{\frac{1}{N-1}\sum_{i=1}^{N} |QT_i - \bar{QT}|^2} \tag{17}$$

4.5. Beat rejection

Automated beat rejection has been applied to exclude unusable heart beats from further QTV analysis (rejection criterion [3] was set to 10% of the median absolute T wave amplitude $\bar{T}_{amp} = median(|T_{amp}|)$ [11]). Heart beats, which show insufficient template adaptation (e.g. spontaneous inversion or biphase of the T wave) will be excluded by this step from further analysis as well.

4.6. Materials

From ECG extracted QTV is a measure of pathophysiological beat-to-beat variations (pathophysiological QTV) and artificial shape variations (artificial QTV) superimposed by signal noise. Because pathophysiological QTV is typically subtle, evaluation of performance considering noise variations is substantial for QTV accuracy. The quantification of artificial QTV (robustness) is done by extracting QTV from noisy ECG signals with no pathophysiological QTV. The validation of pathophysiological QTV (sensitivity) is done by confirming medical findings. Based on previous results [3,19] we compared first the robustness and second the sensitivity of the i2DSW method.

We considered a simulated ECG dataset `Sim` for evaluation of robustness. This dataset has already been used in a comparative study by Baumert et al. [19]. Where three algorithms, template stretch [1], template shift [2] and a conventional (derivative) approach [20] were compared. The outcome showed that template based algorithms outperform conventional methods in most cases. The data provide a good way to characterize a method's behaviour in face of typical problems encountered in QT interval analysis. In this work, previous results obtained by using 2DSW and results of the improved i2DSW method are compared to the results of Baumert et al. [19]. Simulated ECG signals were generated as described previously [20]. By obtaining a noise-free cardiac cycle of an ECG (lead II) that was recorded in a healthy 26 years old volunteer, the ECG was digitized with an A/D board of 12-bit resolution at a sampling rate of 1000 Hz. The T-wave amplitude A_T was scaled by factor k, where $k \in \{0.1, 0.2, 0.3, 0.4, 0.5, 0.6, 0.7, 0.8, 0.9,$

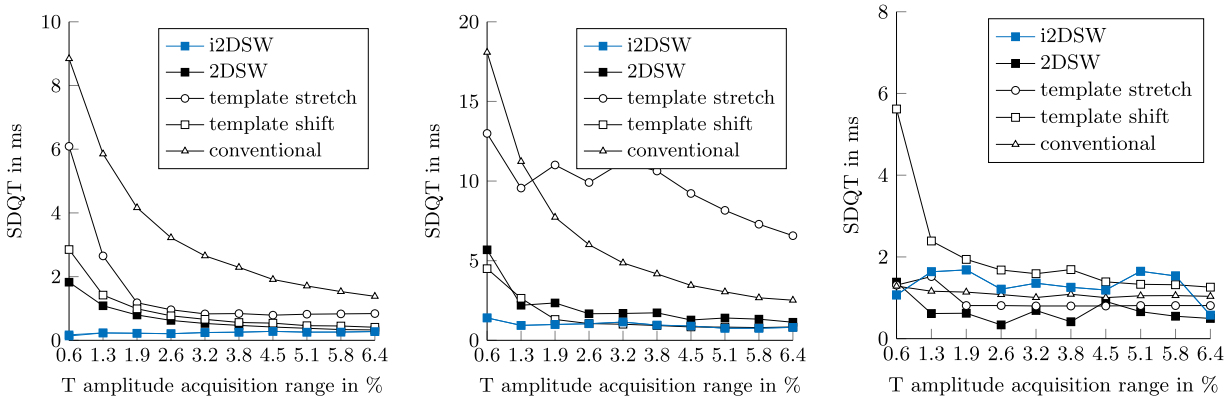

(a) white Gaussian noise. (b) baseline wander. (c) amplitude modulation.

Fig. 5. Results obtained with the i2DSW algorithm in comparison to 2DSW and previously published algorithms using simulated ECG with zero QTV [19]. White Gaussian noise, baseline wander or sinusoidal amplitude modulation were introduced resulting in a total of 30 recordings. Lower QTV values refer to a more accurate measurement.

1.0}, resulting in 10 cardiac beats with decreasing T-wave amplitudes. The 10 cardiac cycles were then repeated 500 times, resulting in ten synthetic signals with 500 cardiac cycles each, characterized by null variability in heart rate and ventricular repolarization duration, but different T wave amplitudes. Additional distortions, namely white Gaussian noise, baseline wander or sinusoidal amplitude modulation of ECG, were introduced resulting in a total of 30 recordings overall. All beats are used for evaluation, beat rejection is not applied for this dataset.

However, as the artificial data do not comprise physiological variations of the QT interval one cannot be able to deduce sensitivity from this test. To assess sensitivity, we used a dataset to measure pathophysiological variations and a clinical trial with circadian variations in QT interval. The PTB Diagnostic ECG Database `PTB` consists of 79 patients with myocardial infarction (MI) (22 female, age: 63 ± 12 years; 57 males, age: 57 ± 10 years) and 69 healthy control subjects (17 females, age: 42 ± 18 years; 52 males, age: 40 ± 13 years) included in the Physikalisch-Technische Bundesanstalt (PTB) diagnostic ECG database [21]. Standard 12-lead ECGs were recorded at a sampling rate of 1000 Hz and a amplitude resolution of 0.5 μV during rest for about 2 min. Previous studies reported higher QTV in MI patients compared to healthy subjects [22,6,23,24]. The present work seeks to compare selected results published in [22] and [6] to the i2DSW results. We compared QTV obtained from lead II in MI patients and healthy controls because significant differences would be expected [24]. Differences between MI patients and healthy controls are assessed by using the Student's *t*-test.

Thorough QT Study `TQT#2` consists of 72 healthy subjects (29 females, age: 47 ± 8 years; 43 males, age: 40 ± 11 years) of the E-HOL-12-0140-008 dataset from the Telemetric and Holter ECG Warehouse (THEW) repository. ECGs were recorded at a sampling rate of 1000 Hz and a amplitude resolution of 3.75 μV in 12-lead Holter ECG configuration. `TQT#2` is a single-dose, randomized, placebo-controlled crossover study. Each subject received a single dose of a randomized treatment or placebo. After 60 min baseline parts (before treatment dosing) a sequence of 23 h of post-dosing is included. By covering 24 h ECG a wide range of heart rates caused by activity and changes in circadian rhythm is expected [24,6]. Moreover, QT morphology variations have been shown by drug induction [25]. Because of that, the `TQT#2` dataset consists of multiple changes in time and morphology of QT interval and in signal quality. To compare the performance of the iterative approach to the standard 2DSW algorithm, we used the ratio of euclidean distance $d^{(2n)}$ after the final adaption between i2DSW and 2DSW

$$d^{(2n)}_{i2DSW:2DSW} = -\left[\frac{d^{(2n)}_{i2DSW}}{d^{(2n)}_{2DSW}} - 1\right]. \tag{18}$$

The 2DSW results for this dataset were based on the version of our algorithm described in [3], but with P-Q extension (see Section 4.2). Therewith, we can apply the same templates to obtain comparable results. No beat rejection has been applied.

Statistical analysis have been performed with IBM SPSS 25. Means of populations have been compared with *t*-test and analysis of variance (ANOVA) [26].

5. Results

Fig. 5 shows the results obtained by applying i2DSW to the `Sim` dataset in comparison to the results presented in [19,3]. i2DSW outperforms the other methods in the categories white Gaussian noise (65% improved compared to 2DSW) and baseline wander (53% improved compared to 2DSW) calculated over all T amplitude acquisition ranges. In the category of amplitude modulation, i2DSW yields higher variations than other algorithms. Taken together, over all noise types and T wave amplitude acquisition ranges, i2DSW improves the results compared to 2DSW by 26% (i2DSW: 0.84 ms; 2DSW: 1.13 ms; template shift: 1.47 ms; template stretch: 4.06 ms; conventional: 3.61 ms). The final adaption over all categories has been improved by more than 60% to $d^{(2n)}_{i2DSW} = 0.22$ μV/sample ($d^{(2n)}_{2DSW} = 0.56$ μV/sample). The maximum iteration cycles are on average 1.0 for white Gaussian noise, 4.0 for baseline wander and 3.7 for amplitude modulation.

Fig. 6 shows the results obtained by applying i2DSW to `PTB` dataset. Beat rejection excluded 0.1% of the beats in healthy subjects and 1.5% of the beats in the MI group. i2DSW results are compared to previous 2DSW results [3] and the results of Hasan et al. [22]. All algorithms show highly significant differences ($p < 0.0001$) between the healthy and the MI group (pairwise testing using Student's *t*-test). A two-way ANOVA (factors: algorithm and population) revealed a significant difference ($p < 0.001$) for the factor population. Qualitatively, i2DSW measures slightly higher QTV than 2DSW.

Fig. 7 shows the ratio between the euclidean distance $d^{(2n)}_{i2DSW:2DSW}$ of i2DSW and 2DSW in relation to the change of heart rate to the template heart rate (ΔHR) for the `TQT#2` dataset. We

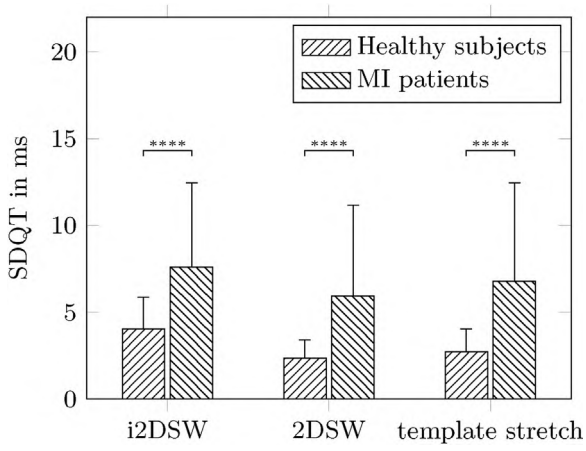

Fig. 6. QTV results obtained with the i2DSW algorithm in comparison to the original 2DSW algorithm [3] and the template stretching method [22] for MI patients and healthy controls (PTB dataset).

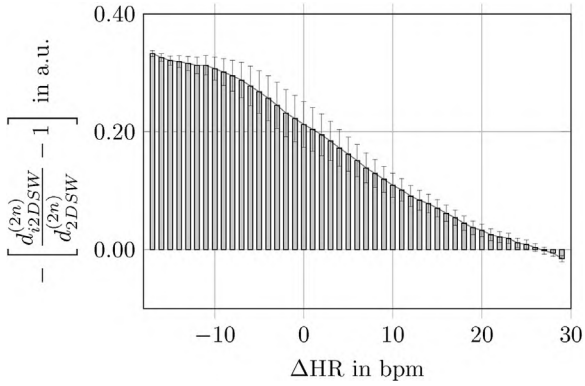

Fig. 7. Ratio of the euclidean distances between template and waveform of i2DSW and 2DSW over the change of heart rate to the template heart rate (ΔHR) for the TQT#2 dataset. The error bars show the normalized number of beats for each ΔHR.

considered only levels of ΔHR that occur in more than 50,000 beats to minimize the influence of outliers (no beat rejection was applied). The curve characteristic shows major improvement for i2DSW (overall $d^{(2n)}_{i2DSW:2DSW} = 0.27$, up to $d^{(2n)}_{i2DSW:2DSW} = 0.33$) for negative ΔHR and minor improvement (overall $d^{(2n)}_{i2DSW:2DSW} = 0.12$, up to $d^{(2n)}_{i2DSW:2DSW} = -0.02$) for positive ΔHR compared to 2DSW. The turning point between positive and negative improvement is between ΔHR = 26 bpm and ΔHR = 27 bpm. Overall, the adaptability of i2DSW is higher ($d^{(2n)}_{i2DSW:2DSW} = 0.19$).

6. Discussion

In this article we presented a novel algorithmic realization of the 2DSW technique with the objective of improving 1D signal adaptation. i2DSW uses an iterative approach to adapt large shape variations more precisely. By avoiding a fixed warping grid segmentation, the template is more flexible and matches subtle variations of shape better than the original realization. Moreover, the template segmentation is independent from signal morphology. Simulation studies showed higher robustness of i2DSW in the presence of typical ECG artefacts. Comparison of short-term ECG recorded in normal subjects versus patients with myocardial infarction (MI) confirmed increased QTV in MI patients. Long-term ECG results showed improved signal adaptation of i2DSW.

6.1. QT evaluation

Test results of Sim dataset show more than 26% improvement in QTV assessment by i2DSW compared to 2DSW. Especially in the case of white Gaussian noise, i2DSW yields the best results. The reason for this improvement is mainly due to the iterative termination. Thus, i2DSW can segment the template in a more adaptive way in respect to the distance $d^{(2n)}$ between template and waveform. In case of amplitude modulation, i2DSW scores slightly higher QTV for some T amplitude acquisition ranges compared to the most other methods. For this case i2DSW reaches the maximum iteration cycles, so the template adaptation is in the most adaptive level of the algorithm. Higher variations, including QT variations, can be possible in a higher degree of adaptation.

The observation of higher QTV in patients with MI [22] could be confirmed by i2DSW in PTB dataset. Similar beat rejection criteria and rejection rates of 2DSW and i2DSW attest to similar final template-to-waveform distance $d^{(2n)}$. Nevertheless, i2DSW measures higher QTV in both groups (healthy and MI). As there is no QTV gold standard available for this dataset, evaluation of absolute QTV values is not feasible. Therefore, relative group differences are more meaningful and have been evaluated ($p < 0.0001$, using Student's t-test).

6.2. Template adaptation

One of the main objectives of the i2DSW algorithm was to improve adaptation in case of large morphological variations. With the generalized iterative design, i2DSW achieved an improvement of more than 60% in the final adaptation in simulated ECG data Sim and 19% in real ECG data TQT#2 with circadian variations. Nevertheless, i2DSW could not improve the results in all cases. With decreasing waveform length ($\Delta HR \geq 26$ bpm in TQT#2) there was a lower adaptivity observed. With respect to QTV assessment, however, it should be noted that a lower (means better) template-to-waveform distance is not a direct measure for more precise QTV assessment. The i2DSW deforming process may differ from ECG waveform morphology variations caused by myocardial cell potentials. Still, the robustness to artificial noise on the one hand and the more flexible adaptation on the other hand showed great advantages of the improved design of i2DSW. Future studies should focus on applying i2DSW to other quasi-periodic signals to test the generalized capabilities of the proposed method.

6.3. Parameterization

To parameterize i2DSW for the application to other types of signals, the initialization of the warping grid and its iteration process are adjustable. The initial number of warping areas $\dot{N}_A$ and the maximum number of iterations $iter_{max}$ define the highest grade of template deforming. To adjust the process of adaptation, different conditions can abort the iteration cycle.

For the application of i2DSW to QTV assessment, parameters are based on the maximum grade of template deforming of 2DSW [11]. To achieve at least the maximum number of warping areas $\tilde{N}_A$ and the maximum number of warping points $\tilde{N}_P$ of i2DSW, $iter_{max}$ was determined as $iter_{max} = 4$ (i2DSW: $\tilde{N}_A = 64$, $\tilde{N}_P = 91$; 2DSW: $N_A = 28$, $N_P = 40$; illustrated in Fig. 8). To avoid overadaptation by allowing a more subtle grid segmentation than 2DSW, combined conditions of absolute changes $\Delta d^{(2n)}$ and relative changes $\Phi d^{(2n)}$ are considered for early iteration cycle termination (see Section 4.3). These conditions are not parameterized by systematic criteria, but based on other parameters in the QTV processing framework, e.g. $\Delta d^{(2n)}$ is oriented at the beat rejection criterion (see Section 4.5) of a mean T wave amplitude of healthy subjects citeschmidt_t_2016

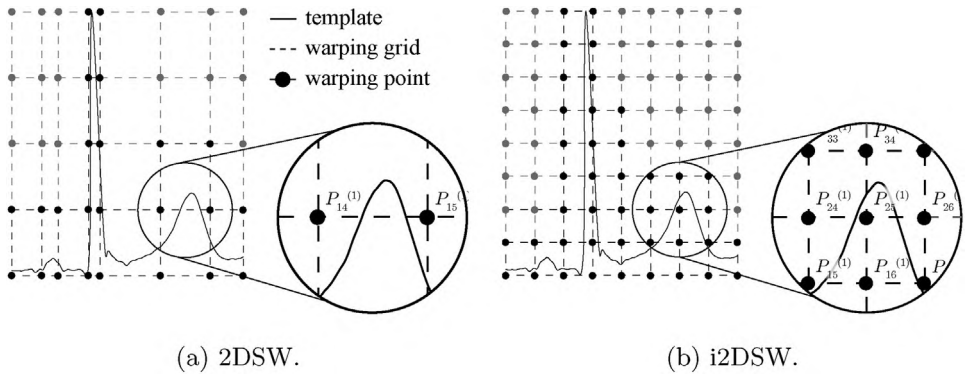

Fig. 8. Grid segmentation schematic of 2DSW (a) and the fourth iteration (final grid segmentation: $iter_{max} = 4$) of i2DSW (b). i2DSW allows in the highest grade of segmentation a higher template deforming process compared to 2DSW.

$(\Delta d^{(2n)}_{(iter)} \ll 30\,\mu V/\text{sample})$. The results demonstrate a more subtle template adaptation (TQT#2) of i2DSW compared to 2DSW. Nevertheless, i2DSW is more robust to noise (Sim) and can measure well-known differences between patient groups of clinical interest (PTB). Taken together, the chosen parameterization seems to be suitable for the application of QTV.

7. Conclusion

The iterative two-dimensional warping approach introduced in this paper is able to detect subtle changes in noisy ECG signals and outperforms established algorithms. We demonstrated its performance in ECG processing by measuring beat-to-beat QT interval variability in simulated and clinical data. The generalized design of i2DSW, i.e. overcoming the need for signal dependent presegmentation as it was needed previously, might also be powerful when applied to other quasi-periodic signals [27,28].

Conflict of interest

The authors declare that the research was conducted in the absence of any commercial or financial relationships that could be construed as a potential conflict of interest.

Acknowledgment

Dataset E-HOL-12-0140-008 used for this research was provided by the Telemetric and Holter ECG Warehouse of the University of Rochester (THEW), NY. This study was partly supported by grants from the Australian Research Council (DP 110102049), Group of Eight Australia and the German academic exchange service (DAAD). We thank the ZIH of the TU Dresden for providing computational power.

References

[1] R.D. Berger, E.K. Kasper, K.L. Baughman, E. Marban, H. Calkins, G.F. Tomaselli, Beat-to-beat QT interval variability: novel evidence for repolarization lability in ischemic and nonischemic dilated cardiomyopathy, Circulation 96 (5) (1997) 1557–1565, http://dx.doi.org/10.1161/01.CIR.96.5.1557.

[2] V. Starc, T.T. Schlegel, Real-time multichannel system for beat-to-beat QT interval variability, J. Electrocardiol. 39 (4) (2006) 358–367, http://dx.doi.org/10.1016/j.jelectrocard.2006.03.004.

[3] M. Schmidt, M. Baumert, A. Porta, H. Malberg, S. Zaunseder, Two-dimensional warping for one-dimensional signals—conceptual framework and application to ECG processing, IEEE Trans. Signal Process. 62 (21) (2014) 5577–5588, http://dx.doi.org/10.1109/TSP.2014.2354313.

[4] J.-P. Couderc, W. Zareba, S. McNitt, P. Maison-Blanche, A.J. Moss, Repolarization variability in the risk stratification of MADIT II patients, Europace 9 (9) (2007) 717–723, http://dx.doi.org/10.1093/europace/eum131.

[5] J. Ramírez, M. Orini, A. Mincholé, V. Monasterio, I. Cygankiewicz, A.B. de Luna, J.P. Martínez, E. Pueyo, P. Laguna, T-wave morphology restitution predicts sudden cardiac death in patients with chronic heart failure, J. Am. Heart Assoc. 6 (5) (2017) e005310, http://dx.doi.org/10.1161/JAHA.116.005310.

[6] M. Schmidt, M. Baumert, H. Malberg, S. Zaunseder, QT interval extraction by two-dimensional signal warping, Biomed. Eng.-Biomed. Tech. 59 (2014) S170–S173.

[7] S. Zaunseder, M. Schmidt, H. Malberg, M. Baumert, Measurement of QT variability by two-dimensional warping, 2014 8th Conference of the European Study Group on Cardiovascular Oscillations (ESGCO) (2014) 163–164, http://dx.doi.org/10.1109/ESGCO.2014.6847570.

[8] M. Baumert, B. Czippelova, A. Ganesan, M. Schmidt, S. Zaunseder, M. Javorka, Entropy analysis of RR and QT interval variability during orthostatic and mental stress in healthy subjects, Entropy 16 (12) (2014) 6384–6393, http://dx.doi.org/10.3390/e16126384.

[9] F. El-Hamad, E. Lambert, D. Abbott, M. Baumert, Relation between QT interval variability and muscle sympathetic nerve activity in normal subjects, Am. J. Physiol.-Heart Circ. Physiol. 309 (7) (2015) H1218–H1224, http://dx.doi.org/10.1152/ajpheart.00230.2015.

[10] M. Baumert, M. Schmidt, S. Zaunseder, A. Porta, Effects of ECG sampling rate on QT interval variability measurement, Biomed. Signal Process. Control 25 (Suppl. C) (2016) 159–164, http://dx.doi.org/10.1016/j.bspc.2015.11.011.

[11] M. Schmidt, M. Baumert, H. Malberg, S. Zaunseder, T wave amplitude correction of QT interval variability for improved repolarization lability measurement, Front. Physiol. 7 (2016), http://dx.doi.org/10.3389/fphys.2016.00216.

[12] C. Vidaurre, T.H. Sander, A. Schlögl, BioSig: the free and open source software library for biomedical signal processing, Comput. Intell. Neurosci. (2011), http://dx.doi.org/10.1155/2011/935364.

[13] V.X. Afonso, W.J. Tompkins, T.Q. Nguyen, S. Luo, ECG beat detection using filter banks, IEEE Trans. Biomed. Eng. 46 (2) (1999) 192–202, http://dx.doi.org/10.1109/10.740882.

[14] A. Cabasson, O. Meste, Time delay estimation: a new insight into the Woody's method, IEEE Signal Process. Lett. 15 (2008) 573–576, http://dx.doi.org/10.1109/LSP.2008.2001558.

[15] P. Laguna, R. Jané, P. Caminal, Automatic detection of wave boundaries in multilead ECG signals: validation with the CSE database, Comput. Biomed. Res. 27 (1) (1994) 45–60, http://dx.doi.org/10.1006/cbmr.1994.1006.

[16] P. Laguna, G.B. Moody, J. García, A.L. Goldberger, R.G. Mark, Analysis of the ST-T complex of the electrocardiogram using the Karhunen—Loeve transform: adaptive monitoring and alternans detection, Med. Biol. Eng. Comput. 37 (2) (1999) 175–189, http://dx.doi.org/10.1007/BF02513285.

[17] J.M. Packard, J.S. Graettinger, A. Graybiel, Analysis of the electrocardiograms obtained from 1000 young healthy aviators: ten year follow-up, Circulation 10 (3) (1954) 384–400, http://dx.doi.org/10.1161/01.CIR.10.3.384.

[18] F. Jager, A. Taddei, G.B. Moody, M. Emdin, G. Antolič, R. Dorn, A. Smrdel, C. Marchesi, R.G. Mark, Long-term ST database: a reference for the development and evaluation of automated ischaemia detectors and for the study of the dynamics of myocardial ischaemia, Med. Biol. Eng. Comput. 41 (2) (2003) 172–182, http://dx.doi.org/10.1007/BF02344885.

[19] M. Baumert, V. Starc, A. Porta, Conventional QT variability measurement vs. template matching techniques: comparison of performance using simulated and real ECG, PLOS ONE 7 (7) (2012) e41920, http://dx.doi.org/10.1371/journal.pone.0041920.

[20] A. Porta, G. Baselli, F. Lombardi, S. Cerutti, R. Antolini, M. Del Greco, F. Ravelli, G. Nollo, Performance assessment of standard algorithms for dynamic R-T interval measurement: Comparison between R-Tapex and R-T(end) approach, Med. Biol. Eng. Comput. 36 (1) (1998) 35–42.

[21] R. Bousseljot, D. Kreiseler, A. Schnabel, Nutzung der EKG-Signaldatenbank CARDIOD der PTB über das Internet, Biomed. Tech. Eng. 40 (s1) (2009) 317–318, http://dx.doi.org/10.1515/bmte.1995.40.s1.317.

[22] M.A. Hasan, D. Abbott, M. Baumert, Beat-to-beat QT interval variability and T-wave amplitude in patients with myocardial infarction, Physiol. Meas. 34 (9) (2013) 1075, http://dx.doi.org/10.1088/0967-3334/34/9/1075.
[23] M.A. Hasan, D. Abbott, M. Baumert, S. Krishnan, Increased beat-to-beat T-wave variability in myocardial infarction patients, Biomed. Eng. Biomed. Tech. (2018), http://dx.doi.org/10.1515/bmt-2015-0186.
[24] M. Baumert, A. Porta, M.A. Vos, M. Malik, J.-P. Couderc, P. Laguna, G. Piccirillo, G.L. Smith, L.G. Tereshchenko, P.G.A. Volders, QT interval variability in body surface ECG: measurement, physiological basis, and clinical value: position statement and consensus guidance endorsed by the European Heart Rhythm Association jointly with the ESC Working Group on Cardiac Cellular Electrophysiology, Europace 18 (6) (2016) 925–944., http://dx.doi.org/10.1093/europace/euv405.
[25] T. Baas, ECG based analysis of the ventricular repolarisation in the human heart, Karlsr. Trans. Biomed. Eng. 18 (2012), http://dx.doi.org/10.5445/KSP/1000028834.
[26] M.G. Bulmer, Principles of Statistics, 2nd ed., Dover Publications, New York, 1979.
[27] F. Censi, I. Corazza, E. Reggiani, G. Calcagnini, E. Mattei, M. Triventi, G. Boriani, P-wave variability and atrial fibrillation, Sci. Rep. 6 (2016) 26799, http://dx.doi.org/10.1038/srep26799.
[28] G. Parati, J.E. Ochoa, C. Lombardi, G. Bilo, Assessment and management of blood-pressure variability, Nat. Rev. Cardiol. 10 (3) (2013) 143, http://dx.doi.org/10.1038/nrcardio.2013.1.